Available online at www.sciencedirect.com
SCIENCE DIRECT®
International Journal of Plasticity 21 (2005) 1890–1918
INTERNATIONAL JOURNAL OF Plasticity
www.elsevier.com/locate/ijplas

The Mori–Tanaka method for composite materials with nonlinear interface debonding

H. Tan [a,*], Y. Huang [a], C. Liu [b], P.H. Geubelle [c]

[a] *Department of Mechanical and Industrial Engineering, University of Illinois at Urbana-Champaign, Urbana, IL 61801, USA*
[b] *MST-8, Materials Science and Technology Division, Los Alamos National Laboratory, Los Alamos, NM 87545, USA*
[c] *Department of Aerospace Engineering, University of Illinois at Urbana-Champaign, Urbana, IL 61801, USA*

Received in final revised form 30 June 2004
Available online 15 December 2004

Abstract

We have used the Mori–Tanaka method to study the effect of nonlinear interface debonding on the constitutive behavior of composite material with high particle volume fraction. The interface debonding is characterized by a nonlinear cohesive law determined from the fracture test of the high explosive PBX 9501. Using the example of the composite material with spherical particles subject to hydrostatic tension, we show that the particle size has an important effect on the behavior of the composite material, namely hardening for small particles and softening for large particles. The critical particle size that separates the hardening and softening behavior of the composite material is determined. For the composite material with large particles, the particle/matrix interface may undergo catastrophic debonding, i.e., sudden, dynamic debonding even under static load. The energy release during catastrophic debonding can be very large, thus may trigger the reaction or detonation of high explosives. For the high explosive PBX 9501, the energy release due to catastrophic debonding of coarse (large)

* Corresponding author. Tel.: +1 217 244 4799; fax: +1 217 244 6534.
E-mail address: htan@uiuc.edu (H. Tan).

0749-6419/$ - see front matter © 2004 Elsevier Ltd. All rights reserved.
doi:10.1016/j.ijplas.2004.10.001

particles is equivalent to the free drop of the high explosive from a height of 110 m. This value become much higher, 455 m, once the debonding of fine (small) particle is accounted for.
© 2004 Elsevier Ltd. All rights reserved.

Keywords: Interfacial debonding; Nonlinear behavior; Size effects; Micromechanics; Particulate reinforced material

1. Introduction

Many composite materials have high particle volume fraction, such as metal matrix composite materials reinforced with 48–65% of alumina particles to improve stiffness and wear resistance (Zhou et al., 2004), and solid propellants and high explosives which contain more than 60% (e.g., Kimura and Oyumi, 1998; Ide et al., 1999; Balzer et al., 2004) and 90% (e.g., Bennett et al., 1998; Liu, 2003b) of energetic particles in polymeric binder matrix, respectively. These composite materials have high specific surface (i.e., high interface area per unit volume of the composite material) such that the behavior of particle/matrix interfaces may significantly influence the macroscopic behavior of composite materials. For example, interfacial debonding between matrix and particles is a major damage mechanism that governs nonlinear and anisotropic behavior of the composite material (e.g., Voyiadjis and Allen, 1996). The interfacial debonding also governs fracture of composite materials with high particle volume fraction. The macroscopic crack propagation is mainly along the particles/matrix interface in solid propellants (e.g., Ho and Fong, 1987; Sciammarella and Sciammarella, 1998; Ide et al., 1999), high explosives (e.g., Wiegand and Pinto, 1996; Rae et al., 2002a,b), and some metal matrix composites (Zhou et al., 2004).

The direct consequence of interfacial debonding is the decrease of modulus of the composite material as compared to that with perfect interfacial bonding. For example, the energetic particles (HMX) in the high explosive PBX 9501 have the volume fraction $f = 92.7\%$ (e.g., Bennett et al., 1998; Liu, 2003b) and elastic bulk modulus $K^{\mathrm{p}} = 12.5$ GPa (Zaug, 1998). The binder matrix has the volume fraction of 7.3%, Young's modulus $E^{\mathrm{m}} = 1$ MPa at the low strain rate, Poisson's ratio $\nu^{\mathrm{m}} = 0.499$ (Cady et al., 2000; Mas et al., 2001), and $\mu^{\mathrm{m}} = E^{\mathrm{m}}/[2(1+\nu^{\mathrm{m}})]$ is the shear modulus of the matrix. If the bonding between the particles and matrix were perfect (i.e., no interfacial debonding), the bulk modulus 1.96 GPa for the high explosive PBX 9501 would be

$$\bar{K} = K^{\mathrm{m}} + \frac{f(K^{\mathrm{p}} - K^{\mathrm{m}})}{1 + (1-f)\frac{K^{\mathrm{p}} - K^{\mathrm{m}}}{K^{\mathrm{m}} + 4\mu^{\mathrm{m}}/3}} = 1.96 \text{ GPa}. \tag{1}$$

The above expression is established from both Mori–Tanaka method (e.g., Taya and Chou, 1981; Weng, 1984, 1990; Benveniste, 1987) and generalized self-consistent method (Christensen, 1990; Huang et al., 1995), and is an accurate expression for the bulk modulus of the composite material. However, the experimentally measured Young's modulus of the high explosive PBX 9501 is 1 GPa at the low strain rate, and

the Poisson's ratio is 0.35 (e.g., Olinger and Hopson, 1978; Gray et al., 1998; Wetzel, 1999; Banerjee and Adams, 2003). These give the bulk modulus of PBX 9501 as $\bar{K} = 1.11$ GPa, which is more than 40% lower than the bulk modulus 1.96 GPa given in Eq. (1). Therefore, the interfacial debonding is mainly responsible for this significant difference between the experimental and theoretical bulk moduli (1.11 GPa versus 1.96 GPa). The finite element simulations on the high explosive PBX 9501, assuming perfectly bonded interfaces, also predicted the elastic modulus higher than the experimental data (Banerjee and Adams, 2002).

Another consequence of the interfacial debonding is the particle size effect, which has been repeatedly observed in composite materials with high particle volume fraction. Rae et al. (2002a) observed that the interfacial debonding always starts around large particles in the high explosive PBX 9501. Fleming et al. (1985) and Kimura and Oyumi (1998) showed that the size of energetic particles plays a critical role in the explosiveness of high explosives and solid propellants, respectively. Under the same total volume fraction of particles, a mix of large and small particles gives much higher explosiveness than that with small ones only. These experiments suggest a critical particle size that strongly influences the performance of high explosives. The classical theories of composite materials involve no intrinsic material length (e.g., Budiansky, 1965; Hill, 1965; Mori and Tanaka, 1973; Christensen and Lo, 1979; Christensen, 1990; Huang et al., 1994a,b, 1995; Huang and Hu, 1995), and therefore cannot predict the observed particle size effect (Huang and Li, 2004; Huang et al., 2004; Hwang et al., 2004; Liu and Hu, 2005; Rashid et al., 2004; Wen et al., 2005).

There are extensive experimental studies on composite materials with high particle volume fraction, such as high explosives (e.g., Rae et al., 2002a), solid propellants (e.g., Balzer et al., 2004), and metal matrix composite materials (e.g., Zhou et al., 2004). These experiments usually involve multiple mechanisms of deformation, such as interface debonding, particle cracking, and matrix deformation and tearing. It is difficult to isolate a single mechanism (e.g., interface debonding) from these experiments. Furthermore, the experiments on energetic materials could be potentially hazardous and therefore very expensive. It is desirable to develop computational or analytical models for the fundamental understanding of deformation mechanisms in composite materials with high particle volume fraction since these models can quantitatively characterize the effect of a single mechanism of deformation.

There are some computational models for high explosives and solid propellants (e.g., Bennett et al., 1998; Hackett and Bennett, 2000; Banerjee and Adams, 2002, 2003, 2004), but very few on interface debonding and its effect on the macroscopic behavior. Zhong and Knauss (1997, 1999) used the cohesive-based finite element method to study the dewetting (debonding) process of spherical rigid particles embedded in an elastic rubbery matrix. However, it is difficult for the computational models to capture the large variation of particle size in high explosives and solid propellants. For example, the size of large particles is more than two orders of magnitude larger than the size of small particles in the high explosive PBX 9501. The small particles, however, also contribute significantly to the macroscopic behavior of the high explosive and must be accounted for in computational models. The advanced multiscale simulation methods are needed to capture the deformation of both large

and small particles (e.g., Raghavan et al., 2001; Ghosh et al., 2001; Banerjee and Adams, 2003, 2004; Carrere et al., 2004; Iwamoto, 2004; Raghavan et al., 2004; Raghavan and Ghosh, 2004; Roos et al., 2004; Voyiadjis et al., 2004; Ghosh and Raghavan, submitted for publication; Raghavan and Ghosh, submitted for publication). It is desirable to develop analytical models that account for the effect of interface debonding on the macroscopic behavior of composite materials with both large and small particles.

The linear cohesive zone model for the particle/matrix interface, which gives a linear relation between stress traction and displacement discontinuity across the particle/matrix interface during debonding, has been used in the analytical studies of interface debonding and its effect on the macroscopic behavior of composite materials (Mal and Bose, 1975; Benveniste and Aboudi, 1984; Benveniste, 1985; Achenbach and Zhu, 1989; Pagano and Tandon, 1990; Hashin, 1991a,b, 2002; Qu, 1993; Zhong and Meguid, 1997). The linear cohesive zone model gives an unphysical infinite cohesive energy, and cannot characterize the nonlinear behavior of the interface, such as softening associated with interface debonding. There are very few analytical studies on the effect of nonlinear cohesive law that involves softening. Levy (1996, 2000) studied the special cases of unidirectional composite reinforced by circular fibers of same radius subject to equibiaxial load and uniaxial tension in the fiber direction, respectively. Tan et al. (submitted for publication) established a theoretical framework for particle-reinforced composite materials to incorporate the nonlinear cohesive law for the particle/matrix interface. But their analysis is limited to the dilute solution which only holds for low particle volume fraction.

The objective of this paper is to investigate the effect of nonlinear interface debonding on the macroscopic behavior of composite materials with high volume fraction of particles, such as high explosives and solid propellants. We establish an analytic model that incorporates the nonlinear cohesive law of the particle/matrix interface to establish the constitutive model of the composite material. Such an analytic model avoids the difficulty associated with numerical methods, and is capable of capturing the size effect for particles with very different sizes.

The paper is outlined in the following. Based on the experimental studies of the high explosive PBX 9501, we establish a nonlinear cohesive law for the particle/matrix interface in Section 2. This nonlinear cohesive law involves softening, and can characterize the debonding of particle/matrix interface. The Mori–Tanaka method, which is applicable to composite materials with high particle volume fraction, is adopted in Section 3 to study the effect of interface debonding on the macroscopic behavior of the composite material. In order to illustrate our approach, we present an example of a composite with spherical particles subject to hydrostatic tension. This example captures the effects of particle size and interface debonding, but avoids the complexity of tension/shear coupling in the cohesive law.

The nonlinear macroscopic behavior of composite materials containing particles of the same size is studied in Section 4. For given properties of the particles, matrix and interfaces, different particle sizes may lead to very different behavior of the composite material, namely hardening of the composite for small particles, and softening for large particles. A critical particle size separating the softening and hardening of

the composite material is determined, and the catastrophic debonding of the particle/matrix interface is discussed in Section 5.

In Section 6, we study the macroscopic behavior of composite materials containing two different sized particles because solid propellants and high explosives display a bimodal distribution of particle size (Fleming et al., 1985; Skidmore et al., 1997; Bennett et al., 1998; Hackett and Bennett, 2000). For example, the high explosive PBX 9501 is mixed with coarse particles (radii ~125 μm) and fine particles (radii ~4 μm) with 3:1 volume ratio (Skidmore et al., 1997; Berghout et al., 2002). Results in this section capture the experimentally observed particle size effect on interface debonding (Rae et al., 2002a; Balzer et al., 2004).

The composite materials with particles of many sizes are studied in Section 7. The particle size distribution in the high explosive PBX 9501 is used. It is shown that the analysis including the particle size contribution but not the contribution from the interface cannot address the observed size effect in the composite materials. The bulk modulus predicted by the present analysis accounting for the particle/matrix interface debonding agrees well with the experimental data.

2. Cohesive law for the high explosive PBX 9501

The high explosive PBX 9501 can be viewed as a composite material composed of 92.7 vol% HMX (energetic) crystals and 7.3 vol% of polymeric binder. The polymeric binder consists of 50% Estane and 50% nitroplasticizer. Estane is segmented block copolymer of polyester and polyurethane, with good adhesion properties. Fig. 1(a) shows the microstructure of PBX 9501, which has a very wide spectrum of size distribution of HMX crystals in order to achieve such a high volume fraction. The size distribution of HMX in PBX 9501, as shown in Fig. 1(b), displays a bimodal distribution with average size of large particles around 250 μm and small particles around 8 μm. In fact, PBX 9501 is mixed with coarse particles (radii ~125 μm) and fine particles (radii ~4 μm) with the 3:1 volume ratio (Skidmore et al., 1997; Berghout et al., 2002). The volume fractions of the coarse and fine particles are therefore 69.5 and 23.2 vol%, respectively.

Liu (2003a) and Tan et al. (submitted for publication) used a specially modified compact tension specimen, together with the digital image correlation technique (Chu et al., 1985), to measure the distributions of cohesive stress σ and opening displacement δ ahead of a tensile crack tip in the high explosive PBX 9501. Details of the experiments are not presented in this paper. The relation between the cohesive stress σ and opening displacement δ gives the macroscopic cohesive law for PBX 9501, and is shown in Fig. 2. The ratio of cohesive strength $\sigma_{\max}$ (maximum cohesive stress) to the Young's modulus E is around 1.66×10^{-3}. Since the Young's modulus of PBX 9501 varies from $E = 0.96$ GPa for quasi-static loading (Gray et al., 1998; Bennett et al., 1998; Banerjee and Adams, 2003) to 1.15 GPa for low-strain rate $\dot{\varepsilon} = 0.44\ \text{s}^{-1}$ (Gray et al., 1998), the cohesive strength varies accordingly from $\sigma_{\max} = 1.66$–1.90 MPa. Before the cohesive strength is reached, the macroscopic cohesive law has a very steep rising portion, which corresponds to a very large initial

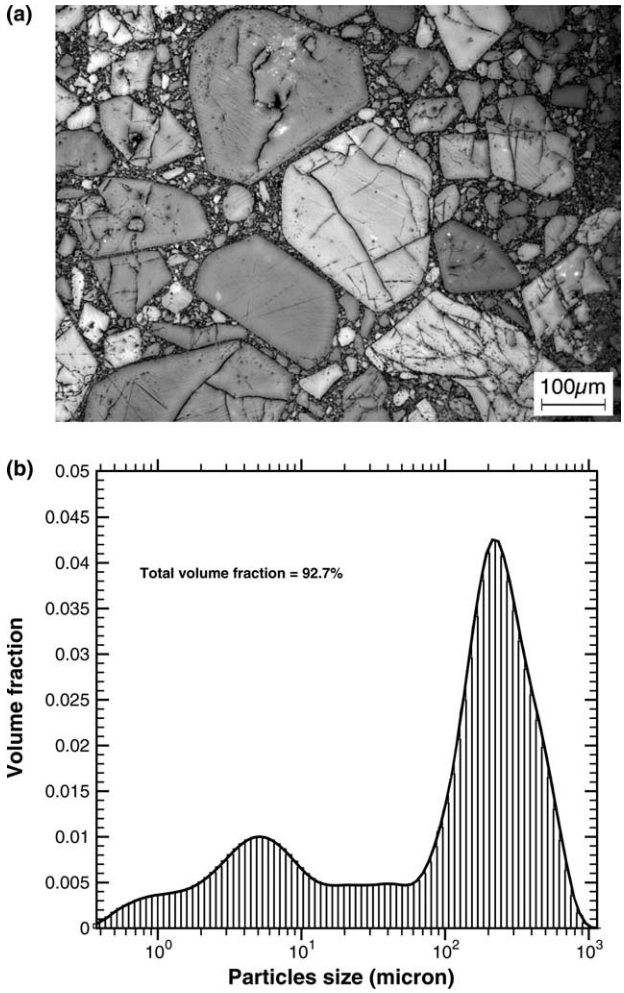

Fig. 1. (a) Micrograph of the high explosive PBX 9501; (b) distribution of particle size in PBX 9501 (courtesy of Cary Skidmore of Los Alamos National Laboratory).

slope around 1.55 GPa/μm. The opening displacement at the cohesive strength is very small, less than 0.2 μm. Once the opening displacement exceeds this value, the cohesive stress decreases (approximately) linearly with the opening displacement, as shown by the straight line in Fig. 2. This straight line has the slope $-0.015\ \mathrm{mm}^{-1}$ in Fig. 2 and its intercept with the horizontal axis is $\delta_c = 0.11$ mm. This intercept represents the critical opening displacement at which the cohesive stress reaches zero and the crack starts to propagate. The cohesive energy (i.e., fracture energy), defined by the total area underneath the $\sigma \sim \delta$ curve, ranges from 85 to 102 $\mathrm{J/m}^2$ for the aforementioned variation of Young's modulus, and it agrees reasonably well with the fracture energy for high explosives reported by Wiegand (1998) and Dienes and Kershner (1998).

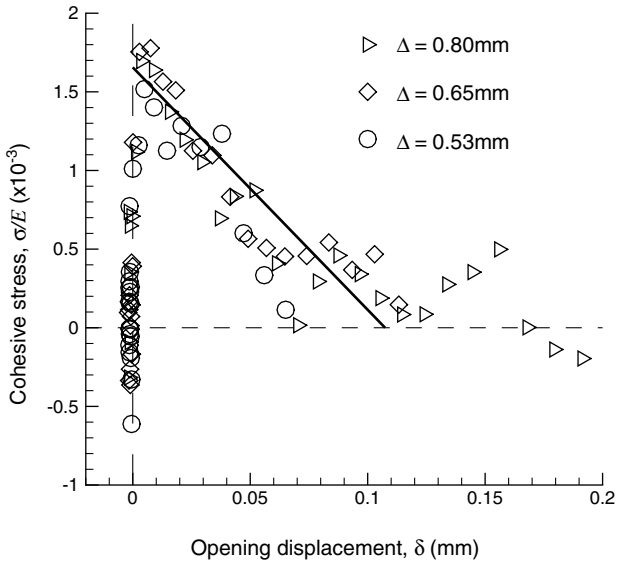

Fig. 2. Cohesive law of the high explosive PBX 9501 under quasi-static loading condition.

It is important to note that we can infer the microscopic cohesive law for the particle/matrix interface from the macroscopic cohesive law in Fig. 2. This is because the high explosive PBX 9501 has a very large particle volume fraction (92.7%) such that the crack propagation in PBX 9501 always follows the particle/matrix interfaces (e.g., Wiegand and Pinto, 1996; Rae et al., 2002a,b). The macroscopic fracture energy is dominated by the particle/matrix interface energy since the contribution from the matrix cracking is negligible. Two key variables in the cohesive law are the opening displacement and the cohesive stress. The opening displacement δ in the macroscopic cohesive law in Fig. 2 is essentially the same as the separation of particle/matrix interfaces on the microscale because the crack always propagates along the interfaces. The cohesive stress at the particle/matrix interface, in general, is different from the macroscopic cohesive stress in Fig. 2. However, as to be shown in the next section, *the difference between the microscopic and macroscopic cohesive stresses is very small* (<0.3%) for the high explosive PBX 9501 because

(i) the elastic modulus of HMX particles is three orders of magnitude larger than that of the polymeric matrix, and the matrix is nearly incompressible;
(ii) the stress field around the tensile crack tip in the modified compact tension experiment has a large stress triaxiality such that its stress state is approximately the hydrostatic tension studied in the next section.

These two conditions ensure that the macroscopic and microscopic stresses are very close. Therefore, the cohesive law measured from the macroscopic fracture test is a good representation of the interface cohesive law for the high explosive PBX 9501.

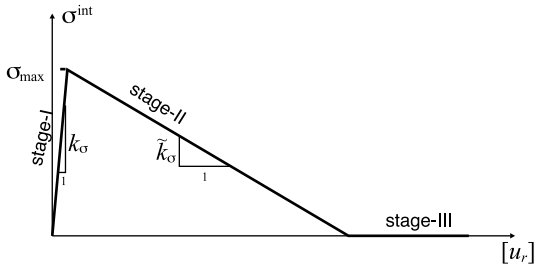

Fig. 3. Interface cohesive model.

As seen from Fig. 2, the rising, descending, and complete debonding portions of the cohesive curve are approximately straight lines, and can be represented by a three-stage (I, II, III), piecewise linear interface cohesive law shown in Fig. 3. This interface cohesive law involves three parameters, namely, the interface cohesive strength $\sigma_{\max}$, and the linear modulus k_σ and softening modulus $\tilde{k}_\sigma$ of the interface, which are the slopes of the rising and descending segments, respectively. The relation between the normal traction σ^{int} and the opening displacement $[u_{\text{r}}]$ at the interface is then given by

$$\begin{aligned}
&\sigma^{\text{int}} = k_\sigma [u_{\text{r}}] && [u_{\text{r}}] < \sigma_{\max}/k_\sigma && \text{stage-I},\\
&\sigma^{\text{int}} = (1 + \tilde{k}_\sigma/k_\sigma)\sigma_{\max} - \tilde{k}_\sigma [u_{\text{r}}] && \sigma_{\max}/k_\sigma < [u_{\text{r}}] < \sigma_{\max}(1/k_\sigma + 1/\tilde{k}_\sigma) && \text{stage-II},\\
&\sigma^{\text{int}} = 0 && [u_{\text{r}}] > \sigma_{\max}(1/k_\sigma + 1/\tilde{k}_\sigma) && \text{stage-III}.
\end{aligned} \tag{2}$$

The interface cohesive energy γ^{int} is related to cohesive strength and linear and softening moduli by $\gamma^{\text{int}} = \frac{\sigma_{\max}^2}{2}(\frac{1}{k_\sigma} + \frac{1}{\tilde{k}_\sigma})$.

3. A micromechanics model accounting for particle/matrix interface debonding: Mori–Tanaka method

3.1. General approach accounting for interface debonding

Tan et al. (submitted for publication) established a theoretical framework to account for the effect of nonlinear interface debonding on the constitutive behavior of composite materials. They also obtained the dilute solution for composite materials with low particle volume fraction. In this section, we use the Mori–Tanaka method to study the *nonlinear* constitutive behavior of composite materials with high particle volume fraction (e.g., solid propellants, high explosives) based on the cohesive law shown in Fig. 3 for the particle/matrix interfaces.

We consider a representative volume element (RVE) of the composite material consisting of particles and matrix. The volume Ω of the RVE is the sum of the matrix

volume Ω^{m} and particle volume Ω^{p}. The particle volume fraction f is given by $\Omega^{\mathrm{p}}/\Omega$. The average stresses in the matrix Ω^{m} and in the particles Ω^{p} are denoted by $\boldsymbol{\sigma}^{\mathrm{m}}$ and $\boldsymbol{\sigma}^{\mathrm{p}}$, respectively. The average stress in the composite $\bar{\boldsymbol{\sigma}}$ is related to $\boldsymbol{\sigma}^{\mathrm{m}}$ and $\boldsymbol{\sigma}^{\mathrm{p}}$ by (e.g., Taya and Chou, 1981; Weng, 1984, 1990; Benveniste, 1987)

$$\bar{\boldsymbol{\sigma}} = (1-f)\boldsymbol{\sigma}^{\mathrm{m}} + f\boldsymbol{\sigma}^{\mathrm{p}}. \tag{3}$$

Similarly, the average strains in the matrix and in the particles are denoted by $\boldsymbol{\varepsilon}^{\mathrm{m}}$ and $\boldsymbol{\varepsilon}^{\mathrm{p}}$, respectively. The average strain in the composite is given by (Tan et al., submitted for publication)

$$\bar{\boldsymbol{\varepsilon}} = (1-f)\boldsymbol{\varepsilon}^{\mathrm{m}} + f\boldsymbol{\varepsilon}^{\mathrm{p}} + f\boldsymbol{\varepsilon}^{\mathrm{int}}, \tag{4}$$

where the additional term $f\boldsymbol{\varepsilon}^{\mathrm{int}}$ represents the contribution from particle/matrix interface debonding (Tan et al., submitted for publication), $\boldsymbol{\varepsilon}^{\mathrm{int}}$ is related to the displacement discontinuity $[\boldsymbol{u}] = \boldsymbol{u}^{\mathrm{m}} - \boldsymbol{u}^{\mathrm{p}}$ across the particle/matrix interface S^{int} by

$$\boldsymbol{\varepsilon}^{\mathrm{int}} = \frac{1}{2\Omega^{\mathrm{p}}}\int_{S^{\mathrm{int}}} ([\boldsymbol{u}]\otimes\boldsymbol{n} + \boldsymbol{n}\otimes[\boldsymbol{u}])\mathrm{d}A, \tag{5}$$

$\boldsymbol{u}^{\mathrm{m}}$ and $\boldsymbol{u}^{\mathrm{p}}$ are the displacements on the interface from the matrix side and particle side, respectively, and $\boldsymbol{n}$ is the unit normal vector on the interface pointing into the matrix.

The particles and matrix are assumed to be linear elastic with the elastic compliance tensors $\boldsymbol{M}^{\mathrm{p}}$ and $\boldsymbol{M}^{\mathrm{m}}$, respectively. Eqs. (3) and (4), together with $\boldsymbol{\varepsilon}^{\mathrm{m}} = \boldsymbol{M}^{\mathrm{m}}:\boldsymbol{\sigma}^{\mathrm{m}}$ and $\boldsymbol{\varepsilon}^{\mathrm{p}} = \boldsymbol{M}^{\mathrm{p}}:\boldsymbol{\sigma}^{\mathrm{p}}$, give the composite strain $\bar{\boldsymbol{\varepsilon}}$ in terms of the composite stress $\bar{\boldsymbol{\sigma}}$ as

$$\bar{\boldsymbol{\varepsilon}} = \boldsymbol{M}^{\mathrm{m}} : \bar{\boldsymbol{\sigma}} + f\left\{(\boldsymbol{M}^{\mathrm{p}} - \boldsymbol{M}^{\mathrm{m}}) : \boldsymbol{\sigma}^{\mathrm{p}} + \boldsymbol{\varepsilon}^{\mathrm{int}}\right\}. \tag{6}$$

For a composite with multi-phase particles, including particles with different sizes, we denote the volume of type-N particles as Ω_N^{p}. Its volume fraction is $f_N = \Omega_N^{\mathrm{p}}/\Omega$. Eqs. (3) and (6) then become

$$\bar{\boldsymbol{\sigma}} = (1-f)\sigma^{\mathrm{m}} + \sum_N f_N\boldsymbol{\sigma}_N^{\mathrm{p}}, \tag{7}$$

$$\bar{\boldsymbol{\varepsilon}} = \boldsymbol{M}^{\mathrm{m}} : \bar{\boldsymbol{\sigma}} + \sum_N f_N\left\{(\boldsymbol{M}_N^{\mathrm{p}} - \boldsymbol{M}^{\mathrm{m}}) : \boldsymbol{\sigma}_N^{\mathrm{p}} + \boldsymbol{\varepsilon}_N^{\mathrm{int}}\right\}, \tag{8}$$

where $f = \sum_N f_N$ is the total particle volume fraction, $\boldsymbol{M}_N^{\mathrm{p}}$ is the elastic compliance tensor of type-N particles, $\boldsymbol{\sigma}_N^{\mathrm{p}}$ is the average stress in type-N particles, $\boldsymbol{\varepsilon}_N^{\mathrm{int}} = \frac{1}{2\Omega_N^{\mathrm{p}}}\int_{S_N^{\mathrm{int}}}([\boldsymbol{u}]\otimes\boldsymbol{n} + \boldsymbol{n}\otimes[\boldsymbol{u}])\mathrm{d}A$, and S_N^{int} is the interface between matrix and type-N particles. It is important to note that Eqs. (7) and (8) are exact. Approximations are made only to evaluate $\boldsymbol{\sigma}^{\mathrm{m}}$, $\boldsymbol{\sigma}_N^{\mathrm{p}}$, and $\boldsymbol{\varepsilon}_N^{\mathrm{int}}$ in terms of the macroscopic stress $\bar{\boldsymbol{\sigma}}$ (or strain $\bar{\boldsymbol{\varepsilon}}$), as discussed in the following.

For perfectly bonded interfaces, i.e., without any debonding, $\boldsymbol{\varepsilon}_N^{\mathrm{int}} = \boldsymbol{0}$ such that only the average stress $\boldsymbol{\sigma}_N^{\mathrm{p}}$ in particles is to be determined in terms of $\bar{\boldsymbol{\sigma}}$ (or $\bar{\boldsymbol{\varepsilon}}$). This is usually accomplished via micromechanics models, such as the Mori–Tanaka method (e.g., Taya and Chou, 1981; Weng, 1984, 1990; Benveniste, 1987). For interfaces with

debonding, both $\boldsymbol{\varepsilon}_N^{\text{int}}$ and $\boldsymbol{\sigma}_N^{\text{p}}$ need to be determined via micromechanics models and the cohesive law for the particle/matrix interface.

3.2. Hydrostatic tension

To illustrate the present approach accounting for the effect of nonlinear interface debonding, we consider an example of an isotropic matrix containing particles subjected to hydrostatic tension $\bar{\sigma}\boldsymbol{I}$, where $\boldsymbol{I}$ is the second-order identity tensor. The particles are also isotropic, and have the same elastic moduli but different sizes denoted by $a_1, a_2, \ldots$ The corresponding volume fraction of particles with size a_N is denoted as f_N. The tensorial equations (7) and (8) then become the following scalar equations

$$\bar{\sigma} = (1-f)\sigma^{\text{m}} + \sum_N f_N \sigma_N^{\text{p}}, \tag{9}$$

$$\bar{\varepsilon}_{kk} = \frac{1}{K^{\text{m}}}\bar{\sigma} + \sum_N f_N \left\{ \left(\frac{1}{K^{\text{p}}} - \frac{1}{K^{\text{m}}}\right)\sigma_N^{\text{p}} + \left(\varepsilon_{kk}^{\text{int}}\right)_N \right\}, \tag{10}$$

where K^{m} and K^{p} are the elastic bulk moduli of the matrix and particles, $\sigma^m = \frac{\sigma_{kk}^{\text{m}}}{3}$ and $\sigma_N^{\text{p}} = \frac{\left(\sigma_{kk}^{\text{p}}\right)_N}{3}$ are the average mean stresses in the matrix and particles, respectively. From Eq. (5), $\langle \varepsilon_{kk}^{\text{int}} \rangle_N$ can be written as

$$\left(\varepsilon_{kk}^{\text{int}}\right)_N = \frac{1}{\Omega_N^{\text{p}}} \int_{S_N^{\text{int}}} [u_n] \mathrm{d}A \tag{11}$$

regardless of the particle shapes, where $[u_{\text{n}}]$ is the displacement discontinuity in the normal direction of the particle/matrix interface. It is important to note that Eqs. (10) and (11) hold for a composite with particles of arbitrary shapes and size distribution.

3.3. Spherical particles of different sizes

For spherical particles with particle radius a_N, Eq. (11) becomes

$$\left(\varepsilon_{kk}^{\text{int}}\right)_N = \frac{1}{\Omega_N^{\text{p}}} \int_{S_N^{\text{int}}} [u_{\text{r}}] \mathrm{d}A = \frac{3[u_{\text{r}}]_N}{a_N}, \tag{12}$$

where $[u_{\text{r}}]_N$ is the average displacement discontinuity in the radial direction on the interfaces between type-N particles and matrix. Therefore, for a composite material with spherical particles, Eq. (10) becomes

$$\bar{\varepsilon}_{kk} = \frac{1}{K^{\text{m}}}\bar{\sigma} + \sum_N f_N \left\{ \left(\frac{1}{K^{\text{p}}} - \frac{1}{K^{\text{m}}}\right)\sigma_N^{\text{p}} + \frac{3[u_{\text{r}}]_N}{a_N} \right\}. \tag{13}$$

For a given cohesive law of the particle/matrix interface, the average displacement discontinuity $[u_r]_N$ can be related to the normal traction σ_N^{int} on the interface, and σ_N^{int} equals the normal stress in the radial direction. We adopt the Mori–Tanaka method to relate σ_N^p and σ_N^{int} to the macroscopic stress $\bar{\sigma}$ (or strain $\bar{\varepsilon}_{kk}$). Eq. (13) then gives the constitutive relation for a composite under hydrostatic tension.

3.4. Mori–Tanaka method

We use the Mori–Tanaka method, which is suitable for composite materials with high particle volume fraction, to determine the average stresses $\boldsymbol{\sigma}_N^p$ in particles and the displacement discontinuities $[u_r]_N$ on the particle/matrix interface in terms of the macroscopic stress $\bar{\sigma}$. The basic idea in the standard Mori–Tanaka method is to relate the average stress $\boldsymbol{\sigma}_N^p$ in particles to the average stress $\boldsymbol{\sigma}^m$ in the matrix (instead of the macroscopic stress $\bar{\boldsymbol{\sigma}}$). This relation, together with Eq. (7), determines $\boldsymbol{\sigma}_N^p$ and $\boldsymbol{\sigma}^m$ in term of $\bar{\boldsymbol{\sigma}}$. For the composite material with particle/matrix interface debonding, the Mori–Tanaka method is modified in the following to incorporate the interface cohesive law in Eq. (2).

Following the standard Mori–Tanaka method, we consider a single spherical particle of radius a_N in an infinite matrix subject to remote hydrostatic stress σ^m, where $\sigma^m = \sigma_{kk}^m/3$ is the average mean stress in the matrix, and it is related to the macroscopic stress $\bar{\sigma}$ and average stress σ_N^p in the particles via Eq. (9). The stress state in the particle is uniform and hydrostatic, and is denoted by $\sigma_N^p \boldsymbol{I}$, where σ_N^p equals to the normal stress σ_N^{int} at the particle/matrix interface. The displacement is discontinuous across the particle/matrix interface due to interface debonding. The radial displacement at the particle boundary is $\frac{\sigma_N^{int}}{3K^p} a_N$. The displacement field in the matrix can be found in Timoshenko and Goodier (1970), and the radial displacement at the inner boundary of the matrix is given in terms of σ^m and σ_N^{int} by $\frac{a_N}{2E^m}\left[3(1-\nu^m)\sigma^m - (1+\nu^m)\sigma_N^{int}\right]$, where E^m and ν^m are the Young's modulus and Poisson's ratio of the matrix, respectively. Therefore, the displacement discontinuity in the radial direction is

$$[u_r]_N = \left(\frac{3(1-\nu^m)\sigma^m - (1+\nu^m)\sigma_N^{int}}{2E^m} - \frac{\sigma_N^{int}}{3K^p}\right) a_N. \tag{14}$$

This equation, in conjunction with the interface cohesive law described in Eq. (2), provides the following relation between σ_N^{int} and σ^m,

$$\begin{aligned} \sigma_N^{int} &= \alpha_N \sigma^m && \text{stage} - \text{I}, \\ \sigma_N^{int} &= \left(1 + \tfrac{\alpha'_N}{\alpha_N}\right)\sigma_{max} - \alpha'_N \sigma^m && \text{stage} - \text{II}, \\ \sigma_N^{int} &= 0 && \text{stage} - \text{III}, \end{aligned} \tag{15}$$

where

$$\alpha_N = \frac{3(1-\nu^m)}{2E^m\left(\frac{1}{k_\sigma a_N} + \frac{1}{3K^p} + \frac{1}{4\mu^m}\right)} \tag{16}$$

and

$$\alpha'_N = -\frac{3(1-\nu^{\mathrm{m}})}{2E^{\mathrm{m}}\left(-\frac{1}{k_\sigma a_N}+\frac{1}{3K^{\mathrm{p}}}+\frac{1}{4\mu^{\mathrm{m}}}\right)} \tag{17}$$

are non-dimensional parameters that depend on not only the properties of particle, matrix, and interface, but also the particle radius a_N. Here α'_N can be written as

$$\alpha'_N = \frac{3\tilde{k}_\sigma(1-\nu^{\mathrm{m}})}{2E^{\mathrm{m}}\left(\frac{1}{a_N}-\frac{1}{a'}\right)}, \tag{18}$$

which is positive for $a_N < a'$ and negative for $a_N > a'$, and

$$a' = \frac{1}{\tilde{k}_\sigma\left(\frac{1}{4\mu^{\mathrm{m}}}+\frac{1}{3K^{\mathrm{p}}}\right)} \tag{19}$$

is a characteristic particle radius. For the high explosive PBX 9501, the bulk modulus of HMX particles $K^{\mathrm{p}} = 12.5$ GPa (Zaug, 1998), Young's modulus of the polymeric matrix $E^{\mathrm{m}} = 1$ MPa (Cady et al., 2000; Mas et al., 2001), Poisson's ratio $\nu^{\mathrm{m}} = 0.499$ (Cady et al., 2000; Mas et al., 2001; Banerjee and Adams, 2003), $\mu^{\mathrm{m}} = E^{\mathrm{m}}/[2(1+\nu^{\mathrm{m}})] = 0.33$ MPa, and linear modulus $k_\sigma = 1.55$ GPa/μm and softening modulus $\tilde{k}_\sigma = 15$ MPa/mm of the interface (based on the slope -0.015 mm^{-1} for the softening portion in Fig. 2 and Young's modulus $E = 1$ GPa for the high explosive PBX 9501). These give the characteristic particle radius in Eq. (19) as $a' = 87$ μm for PBX 9501. It is recalled that the particle size in PBX 9501 follows a bimodal distribution. The average radius of coarse particles is around 125 μm, and is larger than a'. The fine particles have an average radius of 4 μm, and is much less than a'.

Contrary to α'_N, the coefficient α_N in Eq. (16) is always positive. For coarse and fine particles in the high explosive PBX 9501, α_N is 1.0026 and 1.0024, respectively, and is very close to 1. Eq. (15) then give the normal stress at the particle/matrix interface in stage I as $\sigma_N^{\mathrm{int}} = \frac{\alpha_N}{1+\sum_N f_N(\alpha_N-1)}\bar{\sigma} \approx \bar{\sigma}$ for the PBX 9501, i.e., the normal stress at the particle matrix interface is essentially the same as the macroscopic stress. Furthermore, the tensile crack tip fields in Liu's (2003a) and Tan et al.'s (submitted for publication) modified compact tension experiments have large stress triaxialities close to state of hydrostatic tension such that the analysis in this section is applicable, and the above relation $\sigma_N^{\mathrm{int}} \approx \bar{\sigma}$ holds. This is the reason that the microscopic cohesive law in Eq. (2) can be obtained from the macroscopic law in Fig. 2 in Section 2.

Since for spherical particles $\sigma_N^{\mathrm{p}} = \sigma_N^{\mathrm{int}}$, Eq. (9) becomes

$$\bar{\sigma} = (1-f)\sigma_m + \sum_N f_N \sigma_N^{\mathrm{int}}. \tag{20}$$

Eqs. (15) and (20) are the governing equations to determine the average stresses σ^{m} in the matrix and σ_N^{int} at the particle/matrix interface in term of $\bar{\sigma}$.

The macroscopic strain of the composite is obtained in terms of σ^{m} and σ_N^{int} by substituting $[u_{\mathrm{r}}]_N$ in Eq. (14) into Eq. (13),

$$\bar{\varepsilon} = \frac{1}{4\mu^{\mathrm{m}}}\left[\left(\frac{2(1-2\nu^{\mathrm{m}})}{1+\nu^{\mathrm{m}}}+f\right)\sigma^{\mathrm{m}} - \sum_N f_N \sigma_N^{\mathrm{int}}\right], \tag{21}$$

where $\bar{\varepsilon} = \bar{\varepsilon}_{kk}/3$, and Eq. (20) have been used. Since σ^{m} and σ_N^{int} are solved in term of $\bar{\sigma}$ via Eqs. (15) and (20), the above equation gives the macroscopic strain $\bar{\varepsilon}$ in terms of the macroscopic stress $\bar{\sigma}$, i.e., the constitutive relation of the composite material. It is interesting to note that σ_N^{int} and $\bar{\sigma}$ have a linear relation in each stage (see Eq. (15)). Therefore, the stress–strain relation of the composite is piecewise linear.

Once all particles are completely debonded (stage III), i.e., $\sigma_N^{\mathrm{int}} = 0$ for all N, Eq. (21) becomes

$$\bar{\varepsilon} = \frac{1}{4\mu^{\mathrm{m}}(1-f)}\left(\frac{2(1-2\nu^{\mathrm{m}})}{1+\nu^{\mathrm{m}}}+f\right)\bar{\sigma},$$

which corresponds to a straight line in the stress–strain curve. The slope of this straight line corresponds to three times of the elastic bulk modulus

$$\frac{2(1-2\nu^{\mathrm{m}})(1-f)}{2(1-2\nu^{\mathrm{m}})+(1+\nu^{\mathrm{m}})f}K^{\mathrm{m}}$$

of a matrix containing microvoids of volume fraction f predicted by the Mori–Tanaka method. Furthermore, the straight line passes through the origin, $(\bar{\sigma},\bar{\varepsilon}) = (0,0)$, which means that the stress–strain relation becomes identical to that for a matrix containing microvoids, i.e., the gradual debonding process of the particle/matrix interface has no influence once all particles have completely debonded.

For spherical particles embedded in a more compliant matrix, as the case for high explosive PBX 9501, the Mori–Tanaka approach yields Hashin and Shtrikman's (1963) lower bound (Weng, 1984). Recently, Clements and Mas (2001, 2004) and Mas and Clements (2001) developed a constitutive model for plastic bonded explosives based on the theoretical model of Weng and co-workers (Tandon and Weng, 1984; Weng, 1990; Qui and Weng, 1990; Wang and Weng, 1992, 1993; Li and Weng, 1994, 1996a,b, 1997) which has been established from Eshelby's solution of the stress and strain fields in an elastic composite and Mori–Tanaka's effective medium theory. The higher concentration of particles can be modeled by introducing a phenomenological correlation parameter for particle–particle interactions. Such an approach is not adopted in the present study because it is rather difficult to determine this phenomenological correlation parameter in the experiments. Therefore, the particle-particle interaction is only approximately accounted for in the present study via the average stress in the matrix.

4. Particles of the same size

We investigate in this section the composite material with spherical particles of the same radius a. Since the relation between the macroscopic stress $\bar{\sigma}$ and strain $\bar{\varepsilon}$ is piecewise linear (as discussed in the previous section), the stress–strain curve for

Table 1
The macroscopic stress and strain at transition points from stage I to stage II and from stage II to stage III

Transition point	Stages I → II	Stages II → III
Macroscopic stress $\bar{\sigma}$	$[1+f(\alpha-1)]\frac{\sigma_{\max}}{\alpha}$	$(1-f)\frac{2E^{\mathrm{m}}}{3(1-\nu^{\mathrm{m}})}\left(\frac{1}{k_\sigma}+\frac{1}{k_\sigma}\right)\frac{\sigma_{\max}}{a}$ $=(1-f)\frac{4E^{\mathrm{m}}\gamma^{\mathrm{int}}}{3(1-\nu^{\mathrm{m}})\sigma_{\max}a}$
Macroscopic strain $\bar{\varepsilon}$	$\frac{\sigma_{\max}}{2E^{\mathrm{m}}\alpha}[2(1-2\nu^{\mathrm{m}})-f(1+\nu^{\mathrm{m}})(\alpha-1)]$	$\frac{2-4\nu^{\mathrm{m}}+f(1+\nu^{\mathrm{m}})}{3(1-\nu^{\mathrm{m}})}\left(\frac{1}{k_\sigma}+\frac{1}{k_\sigma}\right)\frac{\sigma_{\max}}{a}$ $=\frac{2-4\nu^{\mathrm{m}}+f(1+\nu^{\mathrm{m}})}{3(1-\nu^{\mathrm{m}})}\frac{2\gamma^{\mathrm{int}}}{\sigma_{\max}a}$

the composite material with particles of the same size has three linear segments which correspond to the three stages (I, II, III) of the interface cohesive law (Fig. 3). Therefore, the piecewise linear stress–strain curve is completely determined by the two transition points from stage I to stage II and from stage II to stage III. Table 1 gives the macroscopic stress $\bar{\sigma}$ and strain $\bar{\varepsilon}$ of the composite material at these transition points, which are characterized by the attainment of the cohesive strength $\sigma^{\mathrm{int}}=\sigma_{\max}$ between stages I and II, and $\sigma^{\mathrm{int}}=0$ between stages II and III. The parameter α in Table 1 is α_N in Eq. (16) with the particle radius a_N replaced by a. The incremental bulk moduli for these three stages are given by

$$\bar{K}^{\mathrm{J}}=\frac{2E^{\mathrm{m}}}{3}\frac{1-f+f\alpha^{\mathrm{J}}}{2(1-2\nu^{\mathrm{m}})+f(1-\alpha^{\mathrm{J}})(1+\nu^{\mathrm{m}})},\quad \mathrm{J}=\mathrm{I},\ \mathrm{II},\ \mathrm{III}, \tag{22}$$

where

$$\alpha^{\mathrm{I}}=\frac{3(1-\nu^{\mathrm{m}})}{\frac{2E^{\mathrm{m}}}{k_\sigma a}+\frac{2E^{\mathrm{m}}}{3K^{\mathrm{p}}}+1+\nu^{\mathrm{m}}}$$

is α_N with a_N replaced by a;

$$\alpha^{\mathrm{II}}=\frac{3\tilde{k}_\sigma(1-\nu^{\mathrm{m}})}{2E^{\mathrm{m}}\left(\frac{1}{a'}-\frac{1}{a}\right)}$$

is $-\alpha'_N$ with a_N replaced by a; and $\alpha^{\mathrm{III}}=0$. After all particles debond from the matrix (stage III), $\bar{\sigma}$ and $\bar{\varepsilon}$ are linear and proportional, and are related by

$$\frac{6(1-2\nu^{\mathrm{m}})(1-f)}{2(1-2\nu^{\mathrm{m}})+(1+\nu^{\mathrm{m}})f}K^{\mathrm{m}},$$

which is three times the bulk modulus of the composite material containing microvoids of volume fraction f.

The stress–strain relation predicted by the Mori–Tanaka method is shown in Fig. 4 for the polymeric matrix with 69.5% coarse HMX particles. The matrix is identical to that in the high explosive PBX 9501, and so are the coarse particles which have the same volume fraction and radius (125 μm) as coarse HMX crystals in PBX 9501. However, the effect of fine particles in PBX 9501 is not considered in Fig. 4 since this section is limited to particles of the same size. For comparison, the dilute solution (Tan et al., submitted for publication) for the same composite material is also shown in Fig. 4. It is observed that the two solutions give almost identical stress–strain

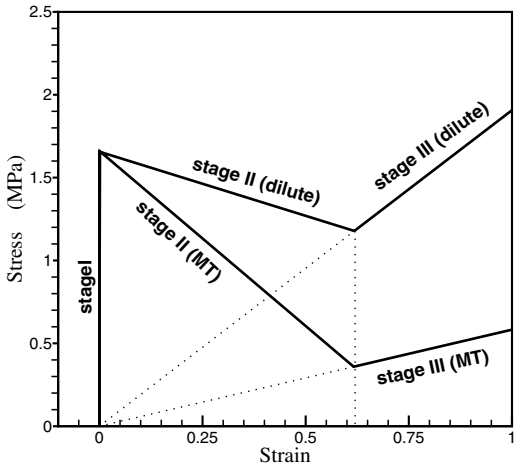

Fig. 4. The stress–strain curve (under hydrostatic tension) of the polymeric matrix with 69.5 vol% coarse HMX particles (radius $a = 125$ μm) predicted by the Mori–Tanaka method. The dilute solution is also shown for comparison.

curves in stage I. The bulk moduli are very large (as compared to the incremental moduli in stages II and III) because the particles are much harder than the matrix ($K^{\mathrm{p}} \gg E^{\mathrm{m}}$) and the matrix is nearly incompressible ($\nu^{\mathrm{m}} \approx 1/2$). In addition, the high linear modulus of the interface ($k_\sigma a \gg E^{\mathrm{m}}$), together with $K^{\mathrm{p}} \gg E^{\mathrm{m}}$ and $\nu^{\mathrm{m}} \approx 1/2$, gives the coefficient α very close to 1 such that the transition points from stage I to stage II given by the Mori–Tanaka method and dilute solution are (almost) identical. If we define the composite strength as the macroscopic stress at the transition point from stage I to stage II (after which the composite material displays softening behavior, Fig. 4), then the dilute solution (Tan et al., submitted for publication) gives rather accurate prediction of the composite strength and linear elastic bulk modulus (at least for the properties of the high explosive PBX 9501). However, once the composite strength is reached, both solutions display softening, and the stress–strain curves become widely separated. The curve for the Mori–Tanaka method decays much faster than that for the dilute solution in stage II. After all particles reach complete debonding, both curves start to increase again (stage III) and their slopes correspond to the bulk moduli given by the Mori–Tanaka method and dilute solution, respectively, for the polymeric matrix with 69.5 vol% microvoids. It is interesting to note that, at the transition points from stage II to stage III the two solutions also give (almost) identical macroscopic strains (at least for the properties of PBX 9501), but Mori–Tanaka method gives a much lower macroscopic stress $\bar{\sigma}^{\mathrm{II}\to\mathrm{III}}$. In fact, $\bar{\sigma}^{\mathrm{II}\to\mathrm{III}}$ by the Mori–Tanaka method is exactly $(1-f)$ times its counterpart in the dilute solution, where f is the particle volume fraction. This reduction (by the factor of $1-f$) is significant for high particle volume fraction.

Fig. 5 shows the stress–strain curve for the polymeric matrix with 23.2 vol% fine HMX particles. The matrix is identical to that in the high explosive PBX 9501, and the particles are also the same as the fine crystals in PBX 9501with radius 4 μm. But

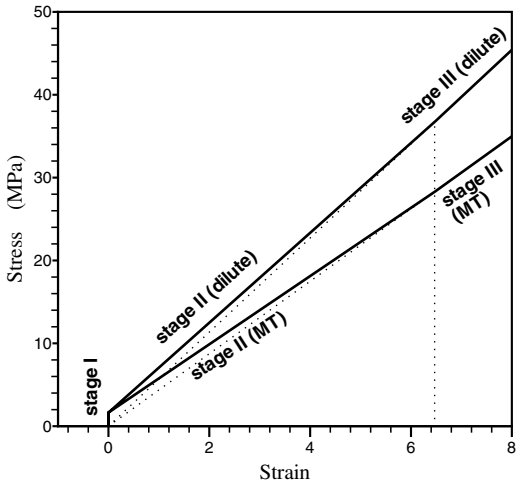

Fig. 5. The stress–strain curve (under hydrostatic tension) of the polymeric matrix with 23.2 vol% fine HMX particles (radius $a = 4$ μm) predicted by the Mori–Tanaka method. The dilute solution is also shown for comparison.

the effect of coarse particles is not considered here. The stress–strain curve given by the dilute solution (Tan et al., submitted for publication) is also shown in Fig. 5 for comparison. Both solutions show the same features as in Fig. 4 except that curves in stage II changes from softening for coarse particles to hardening for fine particles. This suggest that interface debonding can lead to strong particle size effect in the composite material. The Mori–Tanaka method and dilute solution still give (almost) the same transition point between stages I to II, (almost) the same macroscopic strain $\bar{\varepsilon}^{\mathrm{II}\to\mathrm{III}}$, and the macroscopic stresses $\bar{\sigma}^{\mathrm{II}\to\mathrm{III}}$ are still related by the factor $1-f$. The transition point II → III in Fig. 5 is at a unreasonably large strain, which means that small (fine) particles never debond completely (stage III) in reality, but large (coarse) particles do.

The critical particle radius a^{cr} that separates the softening and hardening behavior in stage II of the composite material can be obtained from the incremental bulk modulus $\bar{K}^{\mathrm{II}}$ in Eq. (22), i.e., from $\bar{K}^{\mathrm{II}} = 0$, as

$$a^{\mathrm{cr}} = \frac{1}{\tilde{k}_\sigma}\left[\frac{1}{4\mu^{\mathrm{m}}} + \frac{1}{3K^{\mathrm{p}}} + \frac{f}{1-f}\,\frac{3(1-\nu^{\mathrm{m}})}{2E^{\mathrm{m}}}\right]^{-1}. \tag{23}$$

For particle radius $a < a^{\mathrm{cr}}$, the composite material displays hardening in stage II, while the opposite holds for $a > a^{\mathrm{cr}}$. For the polymeric matrix ($E^{\mathrm{m}} = 1$ MPa, $\nu^{\mathrm{m}} = 0.499$) and HMX particles ($K^{\mathrm{p}} = 12.5$ GPa), the critical particle radius becomes very simple as $a^{\mathrm{cr}} \approx (1-f)a'$, where a' is the characteristic radius given in Eq. (19). With 69.5 vol% coarse particles ($a = 125$ μm) in the polymeric matrix, a^{cr} becomes 27 μm, which is much less than the average radius (125 μm) of coarse particles, but more than that of fine particles ($a = 4$ μm) in the high explosive PBX 9501.

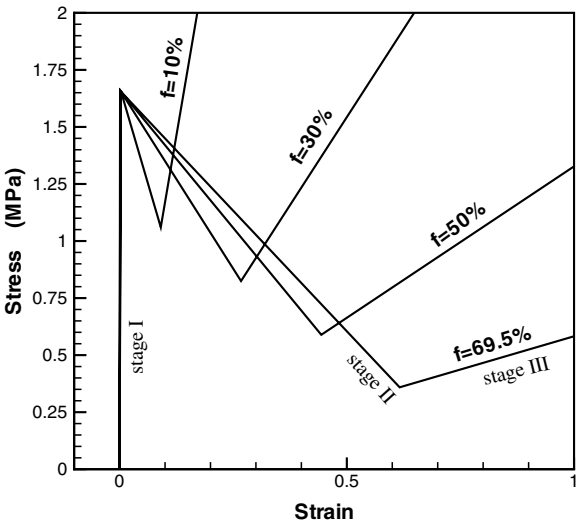

Fig. 6. The stress–strain curve (under hydrostatic tension) of the polymeric matrix with coarse HMX particles ($a = 125$ μm) for several particle volume fraction f.

Therefore, the fine particles lead to hardening of the PBX 9501 while coarse particles do the opposite, i.e., softening. It is noted that the characteristic radius a' in Eq. (19) is a^{cr} for $f \to 0$ (i.e., dilute solution).

Fig. 6 shows the stress–strain curve for the polymeric matrix with only coarse HMX particles and several particle volume fractions ranging from 69.5% (as for the coarse particles in PBX 9501) to 10%. The properties of particles, matrix and interfaces are the same as those in PBX 9501. While all curves coincide in stage I, they are widely separated in stages II and III, indicating a strong dependence on the particle volume fraction. The slope of stage III, in fact, decreases with increasing particle volume fraction f because all particles are completely debonded in stage III and become microvoids.

It is interesting to note the three stages of deformation shown in this section have recently been observed in the tensile tests of biopolymer gel composites (Plucknett et al., 2000a,b; Plucknett and Normand, 2000; Normand et al., 2001) and S-glass/polyurethane composite (Vratsanos and Farris, 1993), as well as in the damage-model simulations of Dvorak and Zhang (2001) and Matous (2003). In particular, these experimental and numerical studies have repeatedly shown that the first and third stages indeed give straight lines that pass through the origin in the stress–strain curve, which is consistent with the present cohesive model prediction.

5. Catastrophic debonding

It has been shown in the previous section that the stress–strain curve may display softening behavior in stage II for large particles. For a composite material with

particle radius $a > a^{cr}$ subject to force-controlled loading, the debonding process will become dynamic once the cohesive strength is reached. As shown in Fig. 7 for the polymeric matrix with 69.5 vol% coarse HMX particles ($a = 125$ μm) under force-controlled loading, the stress–strain curve may bypass the "softening" stage II to reach stage III via the horizontal line marked by II′. Needleman (1987) also observed the dynamic debonding of large particles from the matrix subject to a static load in his cohesive finite element simulations. Such a phenomenon has also been observed in other cohesive finite element simulations (Walter et al., 1997; Zhong and Knauss, 1997; Chaboche et al., 2001). For a polymeric binder matrix that displays strong viscosity as in high explosives and solid propellants (Ho and Fong, 1987; Bandgar et al., 2002; de la Fuente et al., 2003), the inertia effect decays fast such that the composite reaches the equilibrium in stage III rather quickly. The result of dynamic debonding is then represented by the catastrophic jump from stage I to stage III, leading to a sudden (or rapid) increase in the strain (under force-controlled loading). This is called catastrophic debonding in this paper.

The strain increase during the catastrophic jump from stage I to stage III is given by

$$\Delta\bar{\varepsilon} = \frac{\bar{\sigma}^{\mathrm{I}\to\mathrm{II}}}{3}\left(\frac{1}{\bar{K}^{\mathrm{III}}} - \frac{1}{\bar{K}^{\mathrm{I}}}\right) = \frac{f}{1-f}\,\frac{3(1-\nu^{\mathrm{m}})}{2E^{\mathrm{m}}}\,\sigma_{\max}, \tag{24}$$

which is independent of the particle size and properties, and is also independent of the interface cohesive law except the cohesive strength $\sigma_{\max}$. As compared to the dilute solution (Tan et al., submitted for publication) which gives $\Delta\bar{\varepsilon} = f\frac{3(1-\nu^{\mathrm{m}})}{2E^{\mathrm{m}}}\sigma_{\max}$,

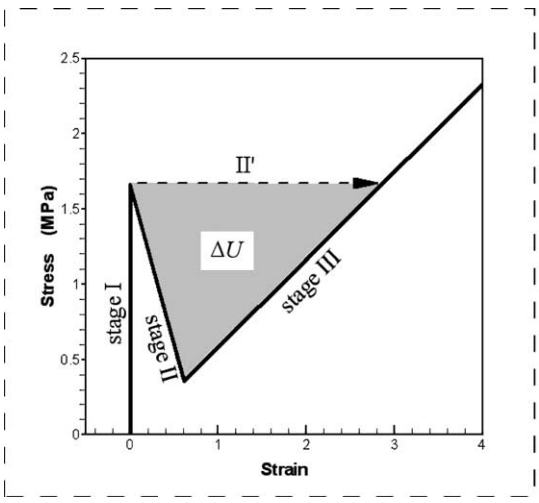

Fig. 7. Catastrophic debonding of the particle/matrix interface under force-controlled loading for the polymeric matrix with 69.5 vol% coarse HMX particles. Here I, II, and III correspond to stages I, II and III, and II′ corresponds to catastrophic debonding.

the strain increase during catastrophic debonding is amplified by a factor $1/(1-f)$, which can be large for high particle volume fraction.

The energy release per unit volume of the composite during catastrophic debonding is represented by the shaded area in Fig. 7, and is given by

$$\Delta U = \frac{\Delta\bar{\varepsilon}}{2}\left(\bar{\sigma}^{\mathrm{I}\to\mathrm{II}} - \bar{\sigma}^{\mathrm{II}\to\mathrm{III}}\right) = \frac{1}{2\tilde{k}_\sigma}\left(\frac{1}{a^{\mathrm{cr}}} - \frac{1}{a}\right) f\sigma_{\max}^2 \quad \text{for } a > a^{\mathrm{cr}}, \tag{25}$$

which vanishes at $a = a^{\mathrm{cr}}$, and increases with the particle radius a. The above expression for the sudden energy release ΔU is exactly the same as that for dilute solution (Tan et al., submitted for publication), except that a^{cr} is now given in Eq. (23) and is much smaller than a' in Eq. (19) for the dilute solution. Therefore, the Mori–Tanaka method gives a larger energy release during catastrophic debonding than the dilute solution (Tan et al., submitted for publication).

In order to illustrate the magnitude of this energy release ΔU during catastrophic debonding, we compare ΔU to the energy release during the free drop of the high explosive from a height of h. From $\Delta U = \rho g h$, we find

$$h = \frac{\Delta U}{\rho g} = \frac{f\sigma_{\max}^2}{2\rho g\tilde{k}_\sigma}\left(\frac{1}{a^{\mathrm{cr}}} - \frac{1}{a}\right), \tag{26}$$

where ρ is the mass density, and $g = 9.8\ \mathrm{m/s^2}$ is the gravity acceleration. For the properties of HMX particles ($K^{\mathrm{p}} = 12.5$ GPa), polymeric matrix ($E^{\mathrm{m}} = 1$ MPa, $\nu^{\mathrm{m}} = 0.499$), and interfaces ($\sigma_{\max} = 1.66$ MPa, $\tilde{k}_\sigma = 15\ \mathrm{MPa/mm}$), Fig. 8 shows the equivalent drop height h as a function of particle size a for several values of particle volume fraction f. The mass density is given by $\rho = f\rho^{\mathrm{p}} + (1-f)\rho^{\mathrm{m}}$, where the

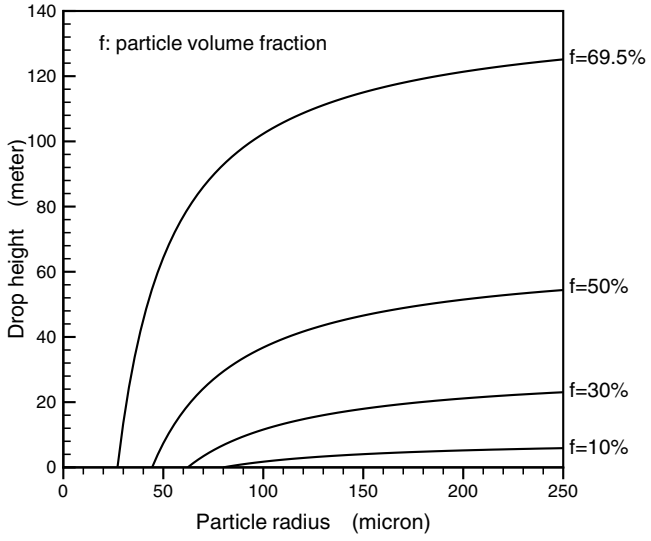

Fig. 8. Equivalent drop height for catastrophic debonding as a function of particle size and volume fraction.

densities of the polymeric matrix and HMX particles are $\rho^{\mathrm{m}} = 1.29 \times 10^3$ kg/m^3 and $\rho^{\mathrm{p}} = 1.90 \times 10^3$ kg/m^3 (Baer et al., 1998), respectively. For the polymeric matrix with 69.5 vol% coarse HMX particles, h is 110 m, which is very large and corresponds to huge energy release due to catastrophic debonding. This sudden energy release may result in the formation of hot spots, which can lead to the reaction or detonation of the high explosive.

6. Particles with two different sizes

We investigate in this section a composite material with spherical particles of two radii, $a_1 > a_2$. The corresponding particle volume fractions are denoted by f_1 and f_2, respectively. The high explosive PBX 9501 represents one such example with $a_1 = 125$ μm, $a_2 = 4$ μm, and $f_1 = 3f_2 = 69.7\%$ (Skidmore et al., 1997; Berghout et al., 2002). The interface cohesive law in Eq. (2) is adopted for the particle/matrix interface. The average stresses σ^{m} in the matrix, σ_1^{int} in coarse particles and σ_2^{int} in fine particles are governed by Eqs. (15) and (20), and the macroscopic strain $\bar{\varepsilon}$ is related to σ^{m}, σ_1^{int} and σ_2^{int} by Eq. (21). However, large particles (a_1) and small ones (a_2) may be on different stages during the deformation. We use a pair of numbers to denote the status of interfaces of large and small particles, and the first number is for large ones. For example, (II,I) stands for large particles in stage II while small particles in stage I.

The stress–strain curve is still piecewise linear, and the incremental bulk modulus of the composite material in each stage is obtained from Eq. (21) by

$$\bar{K}^{(\xi,\eta)} = \left[\frac{1}{K^{\mathrm{m}}} + \frac{9(1-\nu^{\mathrm{m}})}{2E^{\mathrm{m}}}\,\frac{f - f_1\alpha_1^{(\xi)} - f_2\alpha_2^{(\eta)}}{1 - f + f_1\alpha_1^{(\xi)} + f_2\alpha_2^{(\eta)}}\right]^{-1}, \tag{27}$$

where ξ,η = I, II and III, $\alpha_1^{(\xi)} = \alpha_1, -\alpha_1'$ and 0 for ξ = I, II and III, and $\alpha_2^{(\eta)} = \alpha_2, -\alpha_2'$ and 0 for η = I, II and III, respectively, and α_N and α_N' are given in Eqs. (16) and (17). After all particles debond from the matrix [i.e., stage (III,III)], the stress–strain curve becomes a straight line that passes through the origin and has the slope corresponding to three times of the elastic bulk modulus of a matrix containing microvoids with the void volume fraction $f = f_1 + f_2$.

It can be verified from Eq. (15) that large particles reach the cohesive strength first, which is consistent with the experimental observation that large particles debond prior to small ones (e.g., Rae et al., 2002a). Therefore, there exist two patterns of interface debonding,

$$\begin{array}{ll}\text{path 1:} & \\ \text{path 2:} & \end{array} \text{(I,I)} \rightarrow \text{(II,I)} \rightarrow \begin{array}{c}\text{(II,II)}\\ \text{(III,I)}\end{array} \rightarrow \text{(III,II)} \rightarrow \text{(III,III)}, \tag{28}$$

which are named as path 1 and path 2, respectively. Table 2 gives the macroscopic stress $\bar{\sigma}$ for all transition points between any two stages in the flow chart in Eq. (28). The macroscopic strain $\bar{\varepsilon}$ at these transition points can be obtained from Eq. (21), and is not given in Table 2. If small particles reach the cohesive strength

Table 2
The macroscopic stress of the composite material at the transition points between different stages

Transition Point	Macroscopic stress $\bar{\sigma}$
(I,I) → (II,I)	$\frac{\sigma_{\max}}{\alpha_1}(1-f+f_2\alpha_2+f_1\alpha_1)$
(II,I) → (II,II)	$\sigma_{\max}\{\frac{1-f}{\alpha_2}+f+f_1\alpha_1'(\frac{1}{\alpha_1}-\frac{1}{\alpha_2})\}$
(II,II) → (III,II)	$\sigma_{\max}\{(1-f)(\frac{1}{\alpha_1}+\frac{1}{\alpha_1'})+f_2(1-\frac{\alpha_1'}{\alpha_1}-\frac{\alpha_2'}{\alpha_1'}+\frac{\alpha_2'}{\alpha_2})\}$
(III,II) → (III,III)	$\sigma_{\max}(1-f)(\frac{1}{\alpha_2}+\frac{1}{\alpha_2'})$
(II,I) → (III,I)	$\sigma_{\max}(\frac{1}{\alpha_1}+\frac{1}{\alpha_1'})(1-f+f_2\alpha_2)$
(III,I) → (III,II)	$\sigma_{\max}(\frac{1-f}{\alpha_2}+f_2)$

($\sigma_2^{\text{int}} = \sigma_{\max}$) before large particles reach complete debonding ($\sigma_1^{\text{int}} = 0$), then interface debonding takes path 1. On the contrary, path 2 takes place if the complete debonding of large particles ($\sigma_1^{\text{int}} = 0$) occurs prior to the attainment of cohesive strength for small particles ($\sigma_2^{\text{int}} = \sigma_{\max}$).

For the linear modulus to be much larger than the softening modulus of the interface, $k_\sigma \gg \tilde{k}_\sigma$, as for the high explosive PBX 9501, it can be shown that the critical condition to separate paths 1 and 2 is simply

$$\begin{aligned} a_1 < a' &\Rightarrow \text{path 1},\\ a_1 > a' &\Rightarrow \text{path 2}, \end{aligned} \tag{29}$$

i.e., the interface debonding sequence is completely controlled by the size of large particles, and is independent of small ones. The large particles ($a_1 > a'$) reach complete debonding (stage III) while small particles are still in stage I. This is consistent with the experimental observations in composite materials with multi-sized particles, such as in biopolymer gels (Plucknett and Normand, 2000), high explosives (Rae et al., 2002a), and solid propellants (Balzer et al., 2004). These experimental studies have clearly shown that the small particles remain intact when large particles are completely debonded. This has also been observed in the cohesive finite element simulation of particle-filled elastomers (Zhong and Knauss, 2000).

Fig. 9 shows the macroscopic stress–strain relation for the polymeric matrix with 69.5 vol% coarse HMX particles (a_1 = 125 μm) and 23.2 vol% fine HMX particles (a_2 = 4 μm). This composite material is essentially the same as the high explosive PBX 9501, except that the particles have two distinct sizes (125 and 4 μm) instead of the continuous distribution in Fig. 1(b). The stress–strain curve is very steep in stage (I,I), but becomes softening in stage (II,I) after the debonding of coarse particles. Since the radius of coarse particles (a_1 = 125 μm) is larger than a', the coarse particles reach complete debonding while the fine particles are still in stage I [i.e., stage (III,I)] according to Eq. (29). The next stage (III,II), during which fine particles are in the softening stage, gives hardening of the composite material because the radius of fine particles is rather small (4 μm). For comparison, we also show in Fig. 9 the stress–strain curve for the same matrix with coarse particles only (69.5 vol%, a = 125 μm), i.e., to neglect the effect of fine particles. It is interesting to observe that before fine particles reach the softening stage (II), the curves with both coarse and fine particles and with coarse particles only are (almost) identical. This suggests that

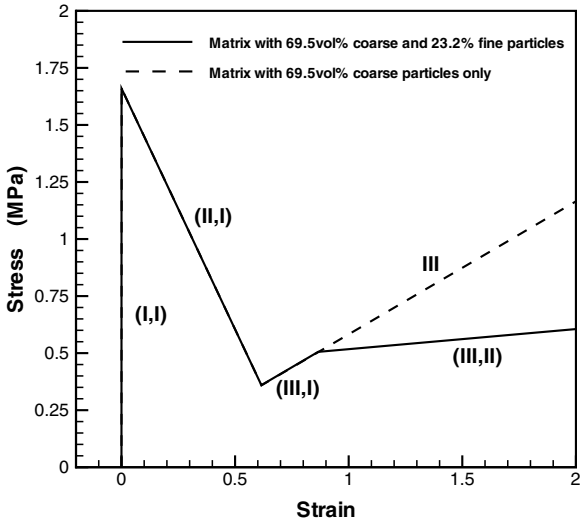

Fig. 9. The stress–strain curve for the plastic bonded explosive with coarse HMX (f_1 = 69.5 vol%, a_1 = 125 μm) and fine HMX particles (f_2 = 23.2%, a_2 = 4 μm). The curve (in dashed line) for the same matrix with coarse particles only (f = 69.5vol%, a = 125 μm) is also shown for comparison.

the fine particles do not contribute to the constitutive behavior of the composite material while they are still in the linear stage I. This is somewhat puzzling, but it has a very simple reason. It is recalled that the particles and interfaces during stage I are much harder than the matrix ($K^{\mathrm{p}} \gg E^{\mathrm{m}}$, $k_\sigma a \gg E^{\mathrm{m}}$), and the matrix is nearly incompressible ($\nu^{\mathrm{m}} \approx 1/2$) such that the composite material is hardly deformed under hydrostatic tension when all particle/matrix interfaces are in stage I, as evidenced by the very steep line for stage (I,I) in Fig. 9. Significant macroscopic strain of the composite material only appears after the interfaces reach the softening stage (II) or complete debonding stage (III). Therefore, the macroscopic strain is dominated by the contribution from interface debonding. When fine particles are in stage I, they hardly contribute to the macroscopic stress–strain curve of the composite material. This is further seen from Fig. 9 which shows that the stage (III,I) curve for the matrix with both coarse and fine particles coincides with the stage III (dashed line) curve for the matrix with coarse particles only. Only when fine particles reach the softening stage, [i.e., (III,II)] the solid line and dashed line start to separate, because fine particles start to make significant contributions to the macroscopic strain.

Fig. 9 also shows that softening behavior of the composite material due to interface debonding of coarse particles. This suggests again the catastrophic debonding under force-controlled load. The energy release during catastrophic debonding becomes much larger than that with coarse particles only because the debonding of fine particles further lowers the stress–strain curve, i.e., from the dashed line to stage (III,II) in Fig. 9. The equivalent free drop height now becomes h = 455 m, and is much larger than h = 110 m given in the previous section that does not account for the fine particles.

7. Particles with many sizes

The particles in the composite material may have many sizes, as shown in the size distribution in Fig. 1(b) for the high explosive PBX 9501. The state of interfaces for all these particles is very complex. In this section we focus on the linear elastic bulk modulus, i.e., when all particle/matrix interfaces are on the linear stage (I). As discussed in Section 1, the Mori–Tanaka method without accounting for the particle/matrix interface debonding overestimates the bulk modulus by over 40% (see Eq. (1)).

The macroscopic strain $\bar{\varepsilon}$ in Eq. (21) now becomes linearly proportional to the macroscopic stress $\bar{\sigma}$ when all particle/matrix interfaces are on stage I. The elastic modulus $\bar{K}$ of the composite material is then obtained from Eqs. (15), (20) and (21) as

$$\bar{K} = \left[\frac{1}{K^{\mathrm{m}}} + \frac{9(1-\nu^{\mathrm{m}})}{2E^{\mathrm{m}}}\,\frac{f - \sum\limits_N f_N \alpha_N}{1 - f + \sum\limits_N f_N \alpha_N}\right]^{-1}, \tag{30}$$

where α_N is given in Eq. (16) and it depends on the particle radius a_N. For the particle size distribution in Fig. 1(b) and the properties of particles ($K^{\mathrm{p}} = 12.5$ GPa), matrix ($E^{\mathrm{m}} = 1$ MPa, $\nu^{\mathrm{m}} = 0.499$) and particle/matrix interfaces ($k_\sigma = 1.55$ GPa/μm), Eq. (30) gives the bulk modulus of the composite material as 1.11 GPa. This value predicted by the present method accounting for interface debonding falls into the range of experimentally determined bulk modulus from 1.07 to 1.27 GPa. Here this range is determined from the experimentally measured Poisson's ratio 0.35 (e.g., Olinger and Hopson, 1978; Gray et al., 1998; Wetzel, 1999; Banerjee and Adams, 2003) and Young's modulus that varies from $E = 0.96$ GPa for quasi-static loading (Gray et al., 1998; Bennett et al., 1998; Banerjee and Adams, 2003) to 1.15 GPa for low-strain rate $\dot{\varepsilon} = 0.44\ \mathrm{s}^{-1}$ (Gray et al., 1998). Therefore, the Mori–Tanaka method accounting for the particle/matrix interface debonding gives reasonable estimate of the bulk modulus of the high explosive PBX 9501.

Eq. (30) gives the bulk modulus $\bar{K}$ of the particulate composite as a function of the elastic constants of the constituents, the properties of the interface between different phases, and the size distribution of the embedding particles. The size of each type of particles appears through the parameter α_N, which has been defined in Eq. (16). Note that the size of the type-N particle, a_N, always appears as the product with the parameter k_σ, which is the linear modulus of the interfacial cohesive law. If the interface between the particle and the matrix is perfectly bonded, i.e., $[\boldsymbol{u}] = 0$, which is equivalent to that $k_\sigma \to \infty$, then the parameter α_N becomes independent of the type-N particle size a_N, and as a matter of fact,

$$\frac{3(1-\nu^{\mathrm{m}})}{2E^{\mathrm{m}}\left(\frac{1}{3K^{\mathrm{p}}} + \frac{1}{4\mu^{\mathrm{m}}}\right)}, \quad \text{for } N = 1, 2, \ldots.$$

One can then show that Eq. (30) degenerates to Eq. (1), and the bulk modulus of the particulate composite $\bar{K}$ depends on the elastic constants of the constituents and the volume fraction of the particle phase only. The conclusion from this observation is that by only including the particle-size distribution in the analysis or simulation without accounting for the contribution from the interface, one cannot address the observed size-effect of the response of composite materials in general, and of high explosives and solid propellants in particular.

8. Discussion and concluding remarks

We have studied the effect of nonlinear interface debonding on the macroscopic behavior of the composite material with high particle volume fraction. Together with a nonlinear cohesive law obtained for the high explosive PBX 9501, the Mori–Tanaka method is used to study the constitutive behavior of the composite material. Using the example of the composite material with spherical particles subject to hydrostatic tension, we show that the particle size has an important effect on the behavior of the composite material, namely hardening for small particles and softening for large particles. The critical particle size that separates the hardening and softening behavior is determined.

For the composite material with large particles, the particle/matrix interfaces may undergo catastrophic debonding, i.e., sudden, dynamic debonding even under static load. The energy release during catastrophic debonding can be very large, thus may trigger the reaction or detonation of high explosives. For the high explosive PBX 9501, the energy release due to catastrophic debonding of coarse (large) particles is equivalent to the free drop of the high explosive from a height of 110 m. This value become much higher, 455 m, once the debonding of fine (small) particle is accounted for.

The above conclusion that the mix of coarse and fine energetic particles gives very high energy release during catastrophic debonding may have important implications on the explosiveness of high explosives (Fleming et al., 1985). A wide range of tests have shown that particle size is an important factor governing the behavior of high explosives (e.g., Balzer et al., 2004). Fleming et al. (1985) studied thoroughly the effects of volume fraction and bimodal size distribution of energetic HMX particles in laboratory-scale explosiveness tests. Here the explosiveness is a measure of the explosive response to a given stimulus. It is measured by the force impressed on the loading cell after explosion. They investigated the explosiveness of the material with fine particles only, and with both fine and coarse particles. Fine particles had a distribution in size, with the maximum radius around 20 μm and average radius around 3.5 μm. Coarse particles ranged from 25 to 500 μm in radius, and the average radius was around 200 μm. Two important observations were made from their experimental studies.

(1) For the high explosive with only fine particles, the explosiveness was not strongly influenced by the particle volume fraction f. Even at a very high f of 96%, the explosiveness was still relatively low.

(2) At the same particle volume fraction f, the use of both coarse and fine particles gave a higher explosiveness than the use of fine particles only. The increase of coarse particle volume fraction (at a fixed total f) led to the increase in the explosiveness.

Similar observations of the particle size effect were also made by Kimura and Oyumi (1998) in the study on shock sensitivity of solid propellants. These observations are consistent with the present study which shows that fine particles, whose radii are less than the critical particle radius a^{cr}, do not have catastrophic debonding to trigger reaction or denotation. The coarse particles do lead to catastrophic debonding, and the energy release is equivalent to the free drop from the height of 110 m. The mix of coarse and fine particles gives even larger energy release during catastrophic debonding that is equivalent to the free drop from a much larger height of 455 m.

Acknowledgements

This research was supported by the US Department of Energy and the US Department of Defense/Office of Land Warfare & Munitions under the Joint DoD/DOE Munitions Technology Development Program, the ASCI Center for Simulation of Advanced Rockets at the University of Illinois supported by US Department of Energy through the University of California under subcontract B523819, and ONR Composites for Marine Structures Program (grants N00014-01-1-0205, Program Manager Dr. Y.D.S. Rajapakse).

References

Achenbach, J.D., Zhu, H., 1989. Effect of interfacial zone on mechanical behavior and failure of fiber-reinforced composites. J. Mech. Phys. Solids 37, 381–393.

Baer, M.R., Kipp, M.E., van Swol, F., 1998. Micromechanical modeling of heterogeneous energetic materials. In: Proceedings of the 11th International Detonation Symposium, Snowmass, Colorado, USA, August 1998, pp. 788–797.

Balzer, J.E., Siviour, C.R., Walley, S.M., Proud, W.G., Field, J.E., 2004. Behaviour of ammonium perchlorate-based propellants and a polymer-bonded explosive under impact loading. Proc. R. Soc. Lond. A 460, 781–806.

Bandgar, B.M., Krishnamurthy, V.N., Mukundan, T., Sharma, K.C., 2002. Mathematical modeling of rheological properties of hydroxyl-terminated polybutadiene binder and dioctyl adipate plasticizer. J. Appl. Polym. Sci. 85, 1002–1007.

Banerjee, B., Adams, D.O., 2002. Micromechanics-based prediction of thermoelastic properties of high energy materials. In: 15th ASCE Engineering Mechanics Conference, June 2–5, 2002, Columbia University, New York, NY, USA.

Banerjee, B., Adams, D.O., 2003. Micromechanics based prediction of effective elastic properties of polymer bonded explosives. Physica B 338, 8–15.

Banerjee, B., Adams, D.O., 2004. On predicting the effective elastic properties of polymer bonded explosives using the recursive cell method. Int. J. Solids Struct. 41, 481–509.

Bennett, J.G., Haberman, K.S., Johnson, J.N., Asay, B.W., Henson, B.F., 1998. A constitutive model for the non-shock ignition and mechanical response of high explosives. J. Mech. Phys. Solids 35, 2303–2322.

Benveniste, Y., 1985. The effective mechanical behaviour of composite materials with imperfect contact between the constituents. Mech. Mater. 4, 197–208.

Benveniste, Y., 1987. A new approach to the application of Mori–Tanaka's theory in composite materials. Mech. Mater. 6, 147–157.

Benveniste, Y., Aboudi, J., 1984. A continuum model for fiber reinforced materials with debonding. Int. J. Solids Struct. 20, 935–951.

Berghout, H.L., Son, S.F., Skidmore, C.B., Idar, D.J., Asay, B.W., 2002. Combustion of damaged PBX 9501 explosive. Thermochim. Acta 384, 261–277.

Budiansky, B., 1965. On the elastic moduli of some heterogeneous materials. J. Mech. Phys. Solids 13, 223–227.

Cady, C.M., Blumenthal, W.R., Gray III, G.T., Idar, D.J., 2000. Mechanical properties of plastic-bonded explosive binder materials as a function of strain-rate and temperature. In: Proceedings of the International Conference on Fundamental Issues and Applications of Shock-Wave and High-Strain-Rate Phenomena (EXPLOMET 2000), Albuquerque, NM.

Carrere, N., Valle, R., Bretheau, T., Chaboche, J.-L., 2004. Multiscale analysis of the transverse properties of Ti-based matrix composites reinforced by SiC fibres: from the grain scale to the macroscopic scale. Int. J. Plasticity 20, 783–810.

Chaboche, J.L., Feyel, F., Monerie, Y., 2001. Interface debonding models: A viscous regularization with a limited rate dependency. Int. J. Solids Struct. 38, 3127–3160.

Christensen, R.M., 1990. A critical evaluation for a class of micro-mechanics models. J. Mech. Phys. Solids 38, 379–404.

Christensen, R.M., Lo, K.H., 1979. Solutions for effective shear properties in three phase sphere and cylinder models. J. Mech. Phys. Solids 27, 315–330.

Chu, T.C., Ranson, W.F., Sutton, M.A., Peters, W.H., 1985. Applications of digital image correlation techniques to experimental mechanics. Experimental Mechanics 25, 232–244.

Clements, B.E., Mas, E.M., 2001. Dynamic mechanical behavior of filled polymers. I. Theoretical developments. J. Appl. Phys. 90, 5522–5534.

Clements, B.E., Mas, E.M., 2004. A theory for plastic-bonded materials with a bimodal size distribution of filler particles. Modelling Simul. Mater. Sci. Eng. 12, 407–421.

Dienes, J.K., Kershner, J.D., 1998. Multiple-shock initiation via statistical crack mechanics. LA-UR-98-3046. In: Proceedings of the 11th International Detonation Symposium, Snowmass, CO, USA, August, pp. 717–724.

Dvorak, G.J., Zhang, J., 2001. Transformation field analysis of damage evolution in composite materials. J. Mech. Phys. Solids 49, 2517–2541.

Fleming, K.A., Bird, R., Burt, M.W.G., Whatmore, C.E., 1985. The influence of formulation variables on the growth of reaction in plastic bonded explosives. In: Short, J.M., Deal, W.E. (Eds.), Proceedings of the 8th International Detonation Symposium, Albuquerque, NM, USA, 15–19 July 1985. Naval Surface Weapons Center, USA, pp. 1035–1044.

de la Fuente, J.L., Fernandez-Garcia, M., Cerrada, M.L., 2003. Viscoelastic behavior in a hydroxyl-terminated polybutadiene gum and its highly filled composites: effect of the type of filler on the relaxation processes. J. Appl. Polym. Sci. 88, 1705–1712.

Ghosh, S., Lee, K., Raghavan, P., 2001. A multi-level computational model for multi-scale damage analysis in composite and porous materials. Int. J. Solids Struct. 38, 2335–2385.

Ghosh, S., Raghavan, P., submitted for publication. Multi-scale model for damage analysis in fiber-reinforced composites with interfacial debonding.

Gray III, G.T., Idar, D.J., Blumenthal, W.R., Cady, C.M., Peterson, P.D., 1998. High- and low-strain rate compression properties of several energetic material composites as a function of strain rate and temperature. In: Proceedings of the 11th International Detonation Symposium, Snowmass, Colorado, USA, 1998, pp. 76–84.

Hackett, R.M., Bennett, J.G., 2000. An implicit finite element material model for energetic particulate composite materials. Int. J. Numer. Methods Eng. 49, 1191–1209.

Hashin, Z., 1991a. Thermoelastic properties of particulate composites with imperfect interface. J. Mech. Phys. Solids 39, 745–762.

Hashin, Z., 1991b. The spherical inclusion with imperfect interface. J. Appl. Mech. 58, 444–449.
Hashin, Z., 2002. Thin interphase/imperfect interface in elasticity with application to coated fiber composites. J. Mech. Phys. Solids 50, 2509–2537.
Hashin, Z., Shtrikman, S., 1963. A variational approach to the elastic behaviour of multiphase materials. J. Mech. Phys. Solids 11, 127–140.
Hill, R., 1965. A self-consistent mechanics of composite materials. J. Mech. Phys. Solids 13, 213–222.
Ho, S.Y., Fong, C.W., 1987. Correlation between fracture properties and dynamic mechanical relaxations in composite propellants. Polymer 28, 739–744.
Huang, Y., Hu, K.X., 1995. A generalized self-consistent mechanics method for solids containing elliptical inclusions. J. Appl. Mech. 62, 566–572.
Huang, M., Li, Z., 2004. Size effects on stress concentration induced by a prolate ellipsoidal particle and void nucleation mechanism. Int. J. Plasticity in press.
Huang, Y., Hu, K.X., Chandra, A., 1994a. A generalized self-consistent mechanics method for microcracked solids. J. Mech. Phys. Solids 42, 1273–1291.
Huang, Y., Hu, K.X., Wei, X., Chandra, A., 1994b. A generalized self-consistent mechanics method for a composite with multi-phase inclusions. J. Mech. Phys. Solids 42, 491–504.
Huang, Y., Hwang, K.C., Hu, K.X., Chandra, A., 1995. A unified energy approach to a class of micromechanics models for composite materials. Acta Mechanica Sinica 11, 59–75.
Huang, Y., Qua, S., Hwang, K.C., Li, M., Gao, H., 2004. A conventional theory of mechanism-based strain gradient plasticity. Int. J. Plasticity 20, 753–782.
Hwang, K.C., Guo, Y., Jiang, H., Huang, Y., Zhuang, Z., 2004. The finite deformation theory of Taylor-based nonlocal plasticity. Int. J. Plasticity 20, 831–839.
Ide, K.M., Ho, S.-Y., Williams, D.R.G., 1999. Fracture behaviour of accelerated aged solid rocket propellants. J. Mater. Sci. 34, 4209–4218.
Iwamoto, T., 2004. Multiscale computational simulation of deformation behavior of TRIP steel with growth of martensitic particles in unit cell by asymptotic homogenization method. Int. J. Plasticity 20, 841–869.
Kimura, E., Oyumi, Y., 1998. Shock instability test for azide polymer propellants. J. Energet. Mater. 16, 173–186.
Levy, A.J., 1996. The effective dilatational response of fiber-reinforced composites with nonlinear interface. J. Appl. Mech. 63, 357–364.
Levy, A.J., 2000. The fiber composite with nonlinear interface-Part I: axial tension. J. Appl. Mech. 67, 727–732.
Li, J., Weng, G.J., 1994. Strain-rate sensitivity, relaxation behavior, and complex moduli of a class of isotropic viscoelastic composites. ASME J. Eng. Mater. Technol. 116, 495–504.
Li, J., Weng, G.J., 1996a. Void growth and stress–strain relations of a class of viscoelastic porous materials. Mech. Mater. 22, 179–188.
Li, J., Weng, G.J., 1996b. Effect of a viscoelastic interphase on the creep and stress/strain behavior of fiber-reinforced polymer matrix composites. Composites, Part B 27B, 589–598.
Li, J., Weng, G.J., 1997. Influence of inclusion microgeometry on some thermomechanical properties of isotropic polymer-matrix composites. ASME J. Eng. Mater. Technol. 119, 242–250.
Liu, C., 2003a. Fracture of the PBX 9501 high explosive. In: Proceedings of 2003 APS Topical Conference on Shock Compression of Condensed Matter, July 20–25, 2003, Portland, Oregon, USA.
Liu, C., 2003b. Specific surface: a missing parameter in high-explosive modeling. LANL Report, LA-14024.
Liu, X., Hu, G., 2005. A continuum micromechanical theory of overall plasticity for particulate composites including particle size effect. Int. J. Plasticity, 777–799.
Mal, A.K., Bose, S.K., 1975. Dynamic elastic moduli of a suspension of imperfectly bonded spheres. Proc. Cambridge Philos. Soc. 76, 587–600.
Mas, E.M., Clements, B.E., 2001. Dynamic mechanical behavior of filled polymers, II. Applications. J. Appl. Phys. 90, 5535–5541.
Mas, E.M., Clements, B.E., Blumenthal, W.R., Cady, C.M., Gray III, G.T., Liu, C., 2001. A viscoelastic model for PBX binders. In: Furnish, M.D., Thadhani, N.N., Horie, Y. (Eds.), Proceedings of the 2001

Conference of the APS Topical Group on Shock Compression of Condensed Matter. American Institute of Physics, Woodbury, New York, pp. 661–664, LA-UR-01-3492.

Matous, K., 2003. Damage evolution in particulate composite materials. Int. J. Solids Struct. 40, 1489–1503.

Mori, T., Tanaka, K., 1973. Average stress in matrix and average elastic energy of materials with misfitting inclusions. Acta Metall. 21, 571–574.

Needleman, A., 1987. A continuum model for void nucleation by inclusion debonding. J. Appl. Mech. 54, 525–531.

Normand, V., Plucknett, K.P., Pomfret, S.J., Ferdinando, D., Norton, I.T., 2001. Large deformation mechanical behavior of gelatin-maltodextrin composite gels. J. Appl. Polym. Sci. 82, 124–135.

Olinger, B., Hopson, J.W., 1978. Dynamic properties of some explosives and explosive simulants. In: Symposium H.D.P., pp. 9–20, Saclay, 1978, Commissariat a l'Energie Atomique.

Pagano, N.J., Tandon, G.P., 1990. Modeling of imperfect bonding in fiber reinforced brittle matrix composites. Mech. Mater. 9, 49–64.

Plucknett, K.P., Normand, V., 2000. Plane stress essential work of fracture of 'pseudo-ductile' gelatin/maltodextrin biopolymer gel composites. Polymer 41, 6833–6841.

Plucknett, K.P., Normand, V., Pomfret, S.J., Ferdinando, D., Frith, W.J., Norton, I.T., 2000a. The influence of interfacial mechanical behaviour upon deformation and fracture of composite biopolymer gels. Mater. Res. Soc. Symp. Proc. 629, FF7.2.1–FF7.2.6.

Plucknett, K.P., Normand, V., Pomfret, S.J., Ferdinando, D., 2000b. 'Ductile' mixed biopolymer gels composites. Polymer 41, 2319–2323.

Qu, J., 1993. The effect of slightly weakened interfaces on the overall elastic properties of composite materials. Mech. Mater. 14, 269–281.

Qui, Y.P., Weng, G.J., 1990. On the application of Mori–Tanaka's theory involving transversely isotropic spheroidal inclusions. Int. J. Eng. Sci. 28, 1121–1137.

Rae, P.J., Goldrein, H.T., Palmer, S.J.P., Field, J.E., Lewis, A.L., 2002a. Quasi-static studies of the deformation and failure of β-HMX based polymer bonded explosives. Proc. R. Soc. Lond. A 458, 743–762.

Rae, P.J., Palmer, S.J.P., Goldrein, H.T., Field, J.E., Lewis, A.L., 2002b. Quasi-static studies of the deformation and failure of PBX 9501. Proc. R. Soc. Lond. A 458, 2227–2242.

Raghavan, P., Ghosh, S., submitted for publication. A continuum damage mechanics model for unidirectional composites undergoing interfacial debonding.

Raghavan, P., Ghosh, S., 2004. Concurrent multi-scale analysis of elastic composites by a multi-level computational model. Comput. Methods Appl. Mech. Engrg. 193, 497–538.

Raghavan, P., Moorthy, S., Ghosh, S., Pagano, N.J., 2001. Revisiting the composite laminate problem with an adaptive multi-level computational model. Comp. Sci. Technol. 61, 1017–1040.

Raghavan, P., Li, S., Ghosh, S., 2004. Two scale response and damage modeling of composite materials. Finite Elements Anal. Design 40, 1619–1640.

Rashid, K., Al-Rub, A., Voyiadjis, G.Z., 2004. Analytical and experimental determination of the material intrinsic length scale of strain gradient plasticity theory from micro- and nano-indentation experiments. Int. J. Plasticity 20, 1139–1182.

Roos, A., Chaboche, J.-L., Gélébart, L., Crépin, J., 2004. Multiscale modelling of titanium aluminides. Int. J. Plasticity 20, 811–830.

Sciammarella, C.A., Sciammarella, F.M., 1998. Investigation of damage in solid propellants. In: Fifth International Conference in Composites Engineering, pp. 779–780.

Skidmore, C.B., Phillips, D.S., Son, S.F., Asay, B.W., 1997. Characterization of HMX particles in PBX 9501. In: Proceedings of the Topical Conference on Shock Compression of Condensed Matter. American Institute of Physics, Los Alamos, NM, pp. 112–119.

Tan, H., Liu, C., Huang, Y., Geubelle, P.H., submitted for publication. The effect of nonlinear interface debonding on the constitutive model of composite materials. Int. J. Multiscale Comput. Eng.

Tandon, G.P., Weng, G.J., 1984. Effect of aspect ratio of inclusions on the elastic properties of unidirectionally aligned composites. Polymer Compos. 5, 327–333.

Taya, M., Chou, T.-W., 1981. On two kinds of ellipsoidal inhomogeneities in an infinite elastic body: an application to a hybrid composite. Int. J. Solids Struct. 17, 553–563.

Timoshenko, S., Goodier, J.N., 1970. Theory of Elasticity, third ed. McGraw-Hill, New York.

Voyiadjis, G.Z., Allen, D.H., 1996. Damage and interfacial debonding in compositesStudies in Applied Mechanics, vol. 44. Elsevier, Amsterdam.

Voyiadjis, G.Z., Rashid, K., Al-Ruba, A., Palazotto, A.N., 2004. Thermodynamic framework for coupling of non-local viscoplasticity and non-local anisotropic viscodamage for dynamic localization problems using gradient theory. Int. J. Plasticity 20, 981–1038.

Vratsanos, V.A., Farris, R.J., 1993. A predictive model for the mechanical behavior of particulate composites-Part I: model derivation. Polym. Eng. Sci. 33, 1458–1465.

Walter, M.E., Ravichandran, G., Ortiz, M., 1997. Computational modeling of damage evolution in unidirectional fiber-reinforced ceramic-matrix composites. Comput. Mech. 20, 192–198.

Wang, Y.M., Weng, G.J., 1992. Influence of inclusion shape on the overall viscoelastic behavior of composites. ASME J. Appl. Mech. 59, 510–518.

Wang, Y.M., Weng, G.J., 1993. Self-similar and transient void growth in viscoelastic media at low concentration. Int. J. Fract. 61, 1–16.

Wen, J., Huang, Y., Hwang, K.C., Liu, C., Li, M., 2005. The modified Gurson model accounting for the void size effect. Int. J. Plasticity, 381–395.

Weng, G.J., 1984. Some elastic properties of reinforced solids, with special reference to isotropic ones containing spherical inclusions. Int. J. Eng. Sci. 22, 845–856.

Weng, G.J., 1990. The overall elastoplastic stress–strain relations of dual-phase metals. J. Mech. Phys. Solids 38, 419–441.

Wetzel, B.J., 1999. Investigation of the creep behaviour of nonlinear viscoelastic simulant materials for high explosives, Diploma thesis, California Institute of Technology, Pasadena, California.

Wiegand, D.A., 1998. Mechanical failure properties of composite plastic bonded explosives. In: Schmidt, D.P., Dandekar, D.P., Forbes, J.W. (Eds.), Shock Compression of Condensed Matter-1997. AIP, Woodbury, NY, pp. 599–602.

Wiegand, D.A., Pinto, J., 1996. The composition of polymer composite fracture surfaces by XPS. Mater. Res. Soc. Symp. Proc. 409, 281–286.

Zaug, J.M., 1998. Elastic constants of β-HMX and tantalum, equations of state of supercritical fluids and fluid mixtures and thermal transport determinations. In: Proceedings of the 11th International Detonation Symposium, Snowmass, Colorado, p. 498.

Zhong, X.A., Knauss, W.G., 1997. Analysis of interfacial failure in particle-filled elastomers. J. Eng. Mater. Technol. 119, 198–204.

Zhong, X.A., Knauss, W.G., 1999. On the stability of phase separation in a finite solid with interfaces. Mech. Compos. Mater. Struct. 6, 1–7.

Zhong, X.A., Knauss, W.G., 2000. Effects of particle interaction and size variation on damage evolution in filled elastomers. Mech. Comp. Mater. Struct. 7, 35–53.

Zhong, Z., Meguid, S.A., 1997. On the elastic field of a spherical inhomogeneity with an imperfectly bonded interface. J. Elasticity 46, 91–113.

Zhou, C.W., Yang, W., Fang, D.N., 2004. Mesofracture of metal matrix composites reinforced by particles of large volume fraction. Theor. Appl. Fract. Mech. 41, 311–326.